Low-THz Dielectric Lens Antenna with Integrated Waveguide Feed

Konstantinidis, Konstantinos; Feresidis, Alexandros; Constantinou, Costas; Hoare, Edward; Gashinova, Marina; Lancaster, Michael; Gardner, Peter

DOI:
10.1109/TTHZ.2017.2725487

Low-THz Dielectric Lens Antenna with Integrated Waveguide Feed

Konstantinos Konstantinidis, Alexandros P. Feresidis, *Senior Member, IEEE*, Costas C. Constantinou, *Member, IEEE*, Edward Hoare, *Senior Member, IEEE*, Marina Gashinova, Michael J. Lancaster, *Senior Member, IEEE* and Peter Gardner, *Senior Member, IEEE*

***Abstract*— A novel dielectric lens antenna with a broadband integrated waveguide-based feed and an optimized tapered extension is presented for low TeraHertz frequencies. The antenna consists of an extended hemispherical lens fed by a standard WR-3 rectangular waveguide fitted directly at the bottom of the lens. The antenna has been designed for high resolution imaging radar systems requiring very wide bandwidth performance and highly directive beams. A novel matching technique based on an air pocket etched off the lens dielectric is employed to obtain broadband antenna operation covering the entire dominant-mode bandwidth of the waveguide. In addition, a new taper shaped lens extension is proposed for the first time and optimized to achieve improved sidelobe level and gain performance. The antenna is compatible with newly developed waveguide-based automotive radar and communications systems. The operating 3dB gain bandwidth is 30% (230GHz - 310GHz) achieving a maximum of 30dB measured gain. The measured S_{11} is well below -14dB across the WR-3 band.**

***Index Terms*— Integrated lens antennas, submillimeter wave, imaging systems**

I. Introduction

TERAHERTZ (THz) frequencies have attracted significant research interest in recent years due to the wide available bandwidth that offers new opportunities. Possible applications in THz include, but are not limited, to communications, sensing and imaging systems [1-3]. Moreover, high-gain, highly efficient and broadband antennas in the region of THz have been subject of investigation over the past few years, since they are required in a number of radar and communications systems. In particular, employing high gain antennas improves the overall system gain compensating for the increased path loss at THz, and thus enhances the signal-to-noise-ratio (SNR). Furthermore, narrow beams and broad bandwidth can provide high spatial and range resolution respectively which are vital characteristics for imaging systems.

Low-THz (300GHz – 1THz) short-range radar imaging systems are being developed for a number of applications including automotive, aerospace etc. Such systems impose a number of requirements on the antennas, specifically, low cost, light weight, vibration robustness and small size antennas as well as the aforementioned performance characteristics.

Nevertheless the implementation of such antennas remains a challenge. Current solutions in the submillimeter-wave band include horn and lens antennas. Planar solutions have also been reported at low-THz for high-gain and beam scanning applications [4, 5]. However, due to the nature of such structures, complex feed networks and fabrication tolerances may cause excessive losses and frequency shift of the operational band. Various implementations of lens antennas have been reported operating at millimeter-wave [6-14] and submillimeter-wave bands [15-28]. In [15, 16], lenses incorporated in THz imaging systems based on CMOS technology with real time capabilities are proposed. Moreover, extended hemispherical lenses and their properties have been extensively investigated [7-9, 17, 20, 21]. This lens shape allows the integration of the primary feed which is a very attractive feature. Multi-shell [11, 12] and arbitrary shape lenses [13, 14] have also been reported. However, at sub-mm wave frequencies the introduction of matching layers and complicated shape designs respectively will demand higher cost and more complex fabrication processes. As reported in [9, 10, 21] extended hemispherical lens antennas with off axis feeding, provide significant advantages in terms of beam scanning applications.

Thus far, efficient illumination of lenses has been a challenge, particularly in those implementations with an integrated primary feed. Feeding techniques that have been employed include dual slots and irises [17-18] as well as more broadband primary sources such as log-spiral and log-periodic feeding antennas [19]. Integrated lenses with waveguide based feeding have been presented for mm-wave frequencies [11, 12]. At sub-mm wave frequencies a silicon lens antenna combined with a half-wavelength Fabry-Perot air cavity has been proposed [20]. However, due to the resonant type feeding technique the operating bandwidth is limited.

In this paper, a broadband THz dielectric lens antenna is proposed, operating from 230GHz to 310GHz, and directly fed by a standard WR-3 rectangular open-ended waveguide. To enable integration with the waveguide feeding source, an extended hemispherical lens type has been chosen. This makes the antenna compatible with newly developed waveguide-

Manuscript received September 28, 2016. "This work was supported by the UK EPRSC under Grant EP/L019078/1".

The authors are with the School of Electronic, Electrical and Systems Engineering, University of Birmingham, Edgbaston, B15 2TT, UK (e-mail: a.feresidis@bham.c.uk).

based automotive radar and communications systems [29]. Different dielectric materials with low dielectric constant values have been considered to avoid the use of a matching layer that significantly increases the fabrication complexity. The antenna achieves broadband operation by means of a novel matching technique based on an air pocket etched off the lens dielectric directly in front of the waveguide aperture. The antenna has been designed to produce highly directive beams required for high resolution imaging radar systems. In order to achieve high directivity over the large operating bandwidth, a tapered extension layer is presented for the first time and optimized for improved gain performance and low sidelobe level. Full-wave simulations have been performed using CST Microwave Studio™ [22] to evaluate the antenna characteristics and demonstrate the effects of the proposed geometries. A prototype of the antenna has been fabricated using CNC milling and experimentally tested to validate the simulated results. Good agreement between the expected and measured performance has been obtained. The maximum measured gain of the proposed antenna is approximately 30dB with an operating 3dB gain bandwidth of 30% (80GHz).

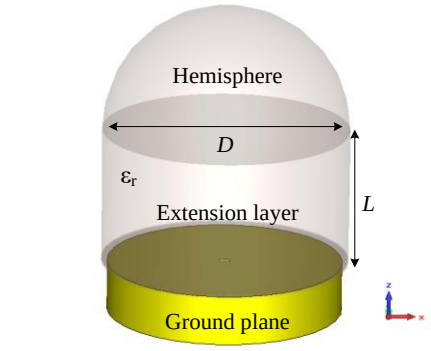

(a)

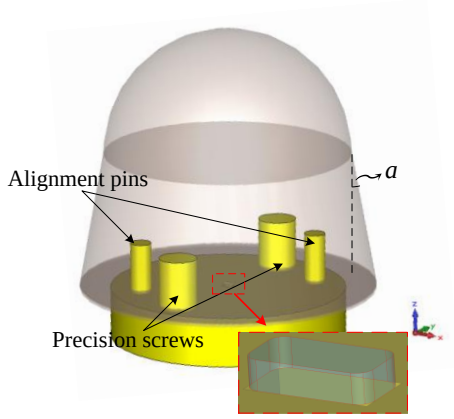

(b)

Fig. 1. (a) Initial geometry of extended hemispherical dielectric lens antenna where ε_r the dielectric constant, D the lens diameter and L the length of the extension layer. (b) Proposed antenna geometry incorporated with the WR-3 flange. A tapering of the extension is performed with a tapering angle α. In the inset an air pocket is shown over the waveguide aperture, with the air presented in blue for better visualization.

The paper is organised as follows: Section II discusses the initial lens antenna design procedure. The design of the broadband waveguide-based feeding technique is presented in Section III. In the same section different dielectric materials are studied and their performances are taken into consideration. Section IV presents the design of the tapered extension layer and its effects on the antenna performance, while Section V discusses the fabrication of the lens prototype. Finally, measurements of the antenna are shown in Section VI.

II. Lens Antenna Design

The initial geometry of the proposed antenna configuration is shown in Fig. 1(a). It consists of a dielectric hemisphere with diameter D and a cylindrical extension layer of the same material and diameter and a length L. The dielectric material that has been used is Rexolite (ε_r=2.53) for reasons that are explained in detail in the next section. The extended hemispherical lens has been chosen to allow integration of the feed antenna. The latter, is a standard WR-3 rectangular open-ended waveguide.

The length of the extension layer is calculated considering that extended hemispherical lenses can be approximated with elliptical lenses [17]. Thus, the length is chosen such that the focal point of the ellipse lies at the bottom of the layer. This approach is an approximation that assumes a point source excitation, which is not true in the case of a waveguide *extended* aperture feed. Hence, a full wave study is carried out in CST Microwave Studio™, taking into account the effect of the primary source pattern in order to select the optimum radius R and the corresponding extension length L. In Fig. 2 the simulated directivity at 290GHz is presented for three different lens radii, as a function of L/R. As expected, the directivity increases with R and obtains its maximum value for $L/R\approx1.1$ for all three cases. This corresponds to an extension length close to the one estimated from the ellipse equation. However, for the case of the smaller lens diameter (R=2.5mm) the variation of the directivity is relatively smooth and becomes sharper as the lens size increases. Consequently for larger lens diameters, careful selection of the extension length is required. Inspection of the radiation patterns for R=5mm and different values of L (Fig. 3) shows that when the feeding is out of focus (i.e. when the extension length is not optimum), high sidelobes occur. The same behavior is exhibited for the lenses with R=2.5mm and 10mm.

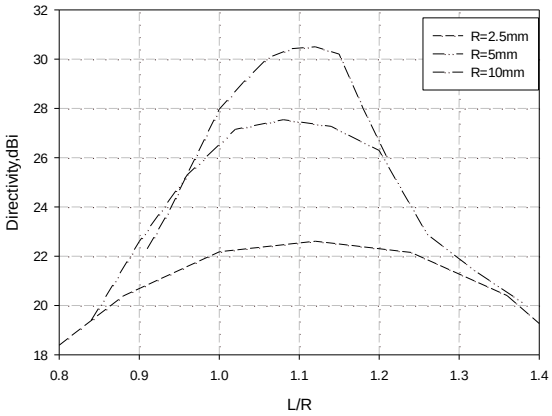

Fig. 2. Directivity as a funcion of the lens extension length at 290GHz for different lens radii: *R*=2.5mm, *R*=5mm and *R*=10mm.

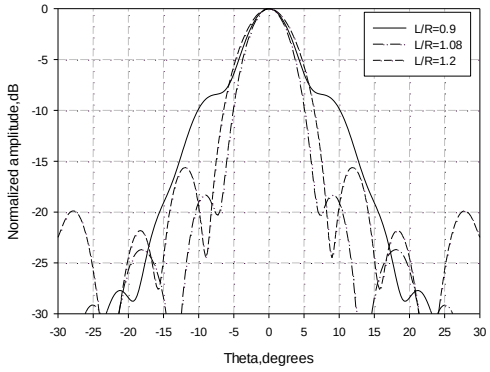

(a)

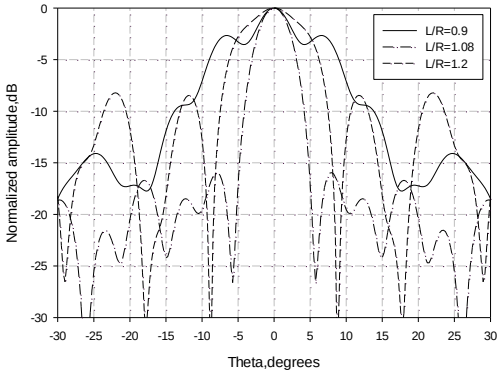

(b)

Fig. 3. Simulated radiation patterns for different extension heights and *R*=5mm at 290GHz (a) H plane, (b) E plane.

III. Broadband Waveguide – Based Feeding

As mentioned in the introduction, the primary feed of the lens antenna is of great importance. The two main considerations when deciding the feeding mechanism for our antenna were firstly, that it can be integrated with our waveguide-based system and secondly, that it produces a broadband matching response. The return loss of the antenna was investigated in CST Microwave Studio and it has been shown that by simply attaching the WR-3 waveguide on the lens extension, the direct interface of the waveguide aperture and the dielectric leads to a poor matching of about −8dB throughout the frequency range of interest (Case A in Fig. 4). To address this issue, a new technique is introduced that produces a broadband matching response.

This technique has been implemented by etching off an air pocket at the bottom of the dielectric lens and directly over the waveguide aperture, as shown in the inset of Fig. 1(b). An air gap over a narrowband patch antenna feeding an extended hemispherical lens has been proposed recently in [30] in order to reduce the sensitivity of the patch impedance and improve the free-space radiation from the primary feed. The proposed matching technique in this paper is based on a rectangular air pocket integrated into the lens, providing a broadband impedance transformation that significantly improves the S_{11} as shown in Fig. 4. Different depths of the air pocket with lateral dimensions equal to those of the waveguide aperture have been studied and are presented in Fig. 4. Cases B, C, E correspond to depths 0.1mm (0.09λ), 0.3mm (0.27λ) and 0.2mm (0.18λ) respectively, showing that the optimum depth is the one of Case E. Finally Case D corresponds to depth 0.2mm, while the length *x* and width *y* of the pocket are increased by 0.2mm. It is evident that the matching is significantly improved in all four Cases (B, C, D and E) while for the optimized pocket dimensions (Case E) the level of the S_{11} response is below −20dB. It should be noted that a reduced frequency range is presented in Fig. 4. This range is chosen to decrease the computational time during the optimization procedure and is also in line with the capabilities of our measurement system (Section VI). Nevertheless, the proposed technique produces a broadband matching covering the complete operating band of the WR-3 waveguide as can be seen in the following section (Fig. 10).

The investigation described above has been carried out considering a Rexolite lens. However, different dielectric materials have also been considered. The S_{11} response for Teflon (ε_r=2.1), Rexolite, PEEK (ε_r=3.2) and Quartz (ε_r=3.75) is shown in Fig. 5. As it can be seen from the graph in all the cases the S_{11} is below -10dB. This demonstrates the applicability of our proposed matching technique on a range of materials that can be used for implementing the lens antenna. However, the higher the permittivity of the dielectric lens the higher the level of S_{11}.

Fig. 6 shows the directivity and radiation patterns at 290GHz for all the materials under consideration. The extension layer length for each material has been optimized for maximum directivity performance for *R*=2.5mm. The directivity and radiation patterns are not affected significantly by changing the dielectric permittivity. The selection criteria for the dielectric lens material are based mainly on the cost and its mechanical and electrical properties at these frequencies. Rexolite offers the required mechanical stability and an extremely low dissipation factor. Moreover, another advantage of Rexolite is that due to its low permittivity value, internal reflections are less pronounced [23, 31]. Finally,

investigations have demonstrated that for materials beyond ε_r=4, anti-reflection coatings are needed on the surface of the hemispherical lens in order to achieve matching for various primary feeds. This imposes significant complications in the fabrication processes, particularly at THz frequencies, and potentially higher cost.

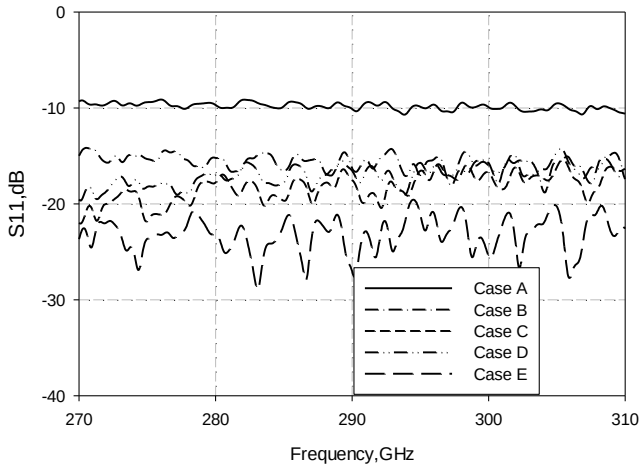

Fig. 4. Simulated input reflection coefficient for pocket thicknesses and sizes.

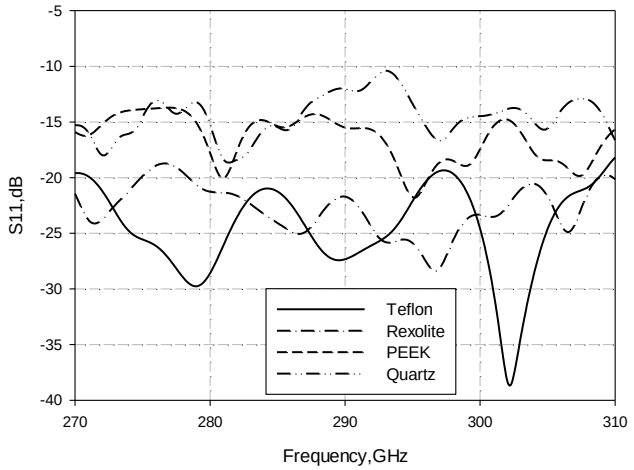

Fig. 5. Simulated input reflection coefficient for different materials.

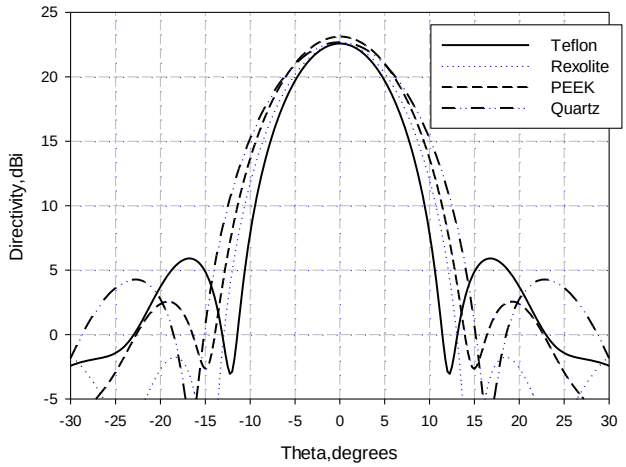

(a)

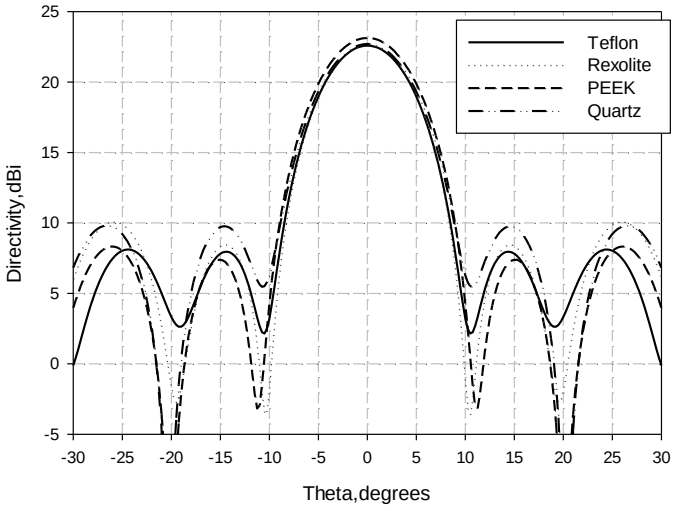

(b)

Fig. 6. Simulated radiation patterns for different materials at 290GHz (a) H plane, (b) E plane.

IV. Tapered Extension Design

So far the geometry of the lens antenna under investigation was the conventional extended hemisphere with a ground plane and an open-ended rectangular waveguide (Fig. 1a). In this section, an optimization of the geometry is performed for a lens with radius R=10mm. This radius is selected to achieve a directivity of more than 30dB which is in accordance with the requirements of our radar system. As explained below, the new geometry shown in Fig. 1(b) derives from a tapering of the extension layer with a certain angle a. At this stage, the complete waveguide flange with its pins and screws is included at the simulations to obtain more accurate results.

In Fig. 7 the directivity as a function of frequency is presented, for several tapering angles at the optimum extension length L/R=1.1 and R=10mm. Initially, in the case of no tapering, i.e. for a=0°, approximately 1.5 dB fluctuation is observed in the directivity response. This is attributed to both the spillover effect due to the high extension length of the

lens and the internal reflections [23, 30]. Recently, modifications to shape of the extension have been reported [32] in order to minimize the internal reflections in an extended hemispherical lens, but the proposed design is complex to manufacture and has been optimized for a scanning array primary feed. In this paper we propose a new, easy to fabricate linear tapering of the extension layer which minimizes the gain fluctuations and increases the directivity level (Fig. 7) over a wide range of frequencies. More particularly, for a=−5.2º, an inward tapering is performed which results in a better performance and less ripples of the directivity. Nevertheless, the inward tapering angle is restricted from the actual flange dimensions, and it cannot be further increased. Hence, an outward tapering is employed. In the optimum case, which corresponds to an outward tapering of a=10.4º, the directivity is increased by more than 2dB compared to the a=0º case. Moreover, the observed fluctuation is significantly reduced. Finally, it should be noticed that for larger tapering angles (a=24.6º) the directivity drops and larger fluctuations are observed. Above a certain tapering angle value, the condition for total internal reflection is not satisfied for the most part of the primary radiation and this leads to a spillover loss.

Another way of showing the benefits of the proposed tapering technique in terms of reduction of the spillover effect is inspecting the radiation patterns. The radiation patterns for three different frequencies within the frequency range of our measurement system are presented in Fig. 8, for the case of the conventional lens (a=0º) and the optimized one (a=10.4º). It should be pointed out that the operating bandwidth of the proposed lens antenna is considerably larger than the one of the radiation patterns measurement system, covering from 230GHz to 320GHz (see Fig. 10). It can be observed that for the optimized case (a=10.4º) an improved sidelobe level is exhibited. More specifically, significant improvement is observed at angles higher than 5º in both planes. Furthermore, the electric field magnitude inside the lens for the initial and the optimum design are illustrated in Fig. 9 for both E- and H-plane. It is evident that for the conventional extended hemispherical lens there is spillover along the edges of the extension layer. It is also worth noting that the hemispherical surface is illuminated in its entirety contributing to the high sidelobe levels. On the other hand, for the tapered design, spillover occurs only at the upper part of the extension and only a reduced part of the hemisphere's upper surface is illuminated. Moreover, considering the surface of the extension as a radiating aperture, tapering introduces a phase gradient along the z-axis which has an optimum value in terms of the maximum directivity as illustrated in Fig. 7.

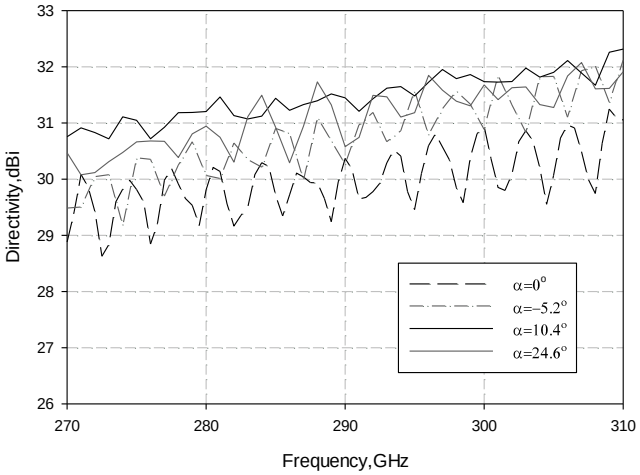

Fig. 7. Simulated directivity versus frequency for different tapering angles.

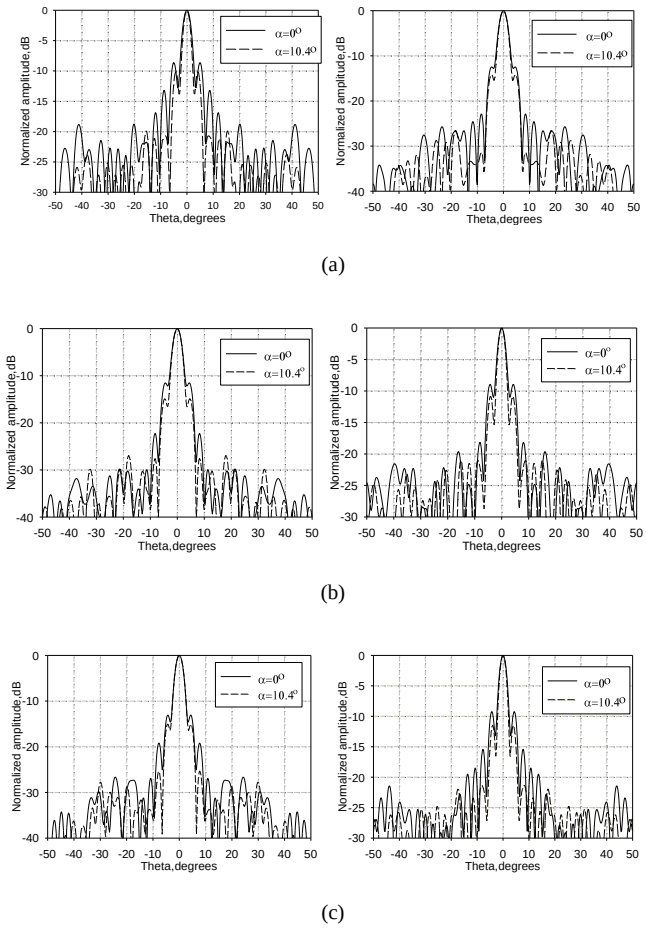

Fig. 8. Simulated normalized radiation patten comparison with and without the tapering technique for (a) 282GHz, (b) 290GHz and (c) 298GHz, H-plane(left), E-plane(right).

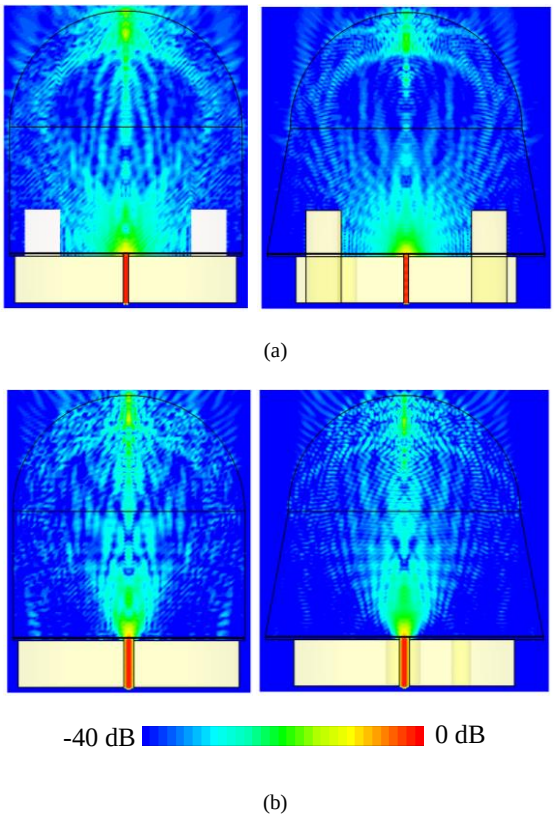

Fig. 9. Magnitude of the electric field inside the lens with and without tapering (a) E-planes and (b) H-planes.

The simulated realized gain and S_{11} of the optimum tapered lens antenna (α=10.4º) from 230GHz to 310GHz is presented in Fig. 10. It is clearly shown that the S_{11} is well below -17dB over the whole frequency range, while the 3dB gain bandwidth is 30% which corresponds to 80GHz bandwidth. Both these characteristics of the proposed lens antenna are of significant interest, especially for low-THz frequencies, since to the best of our knowledge this is the first report of such broadband lens antenna with integrated feeding in terms of both high gain and return loss. Within the 3-dB gain bandwidth, very smooth variation of the beamwidths at both H– and E–planes is observed (Fig. 11). More particularly, the H– and E–plane radiation patterns exhibit a variation of 0.8º and 0.7º respectively from 230GHz to 310GHz. Stable beamwidths with the frequency is an important feature of our current imaging system. In this way, angular resolution will remain constant across the operating bandwidth which will improve the range resolution. The effect of the waveguide flange integration in the lens has also been studied through simulations and the resulting radiation patterns are shown in Fig. 12. It is demonstrated that there is no negative effect from the flange. In fact, the metallic screws contribute positively to ~2dB suppression of sidelobes for angles higher than 8º at both planes.

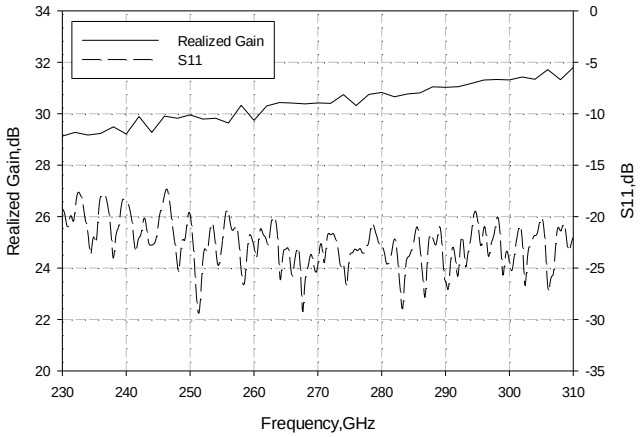

Fig. 10. Simulated S_{11} and realized gain of the optimum tapered lens design (α=10.4º).

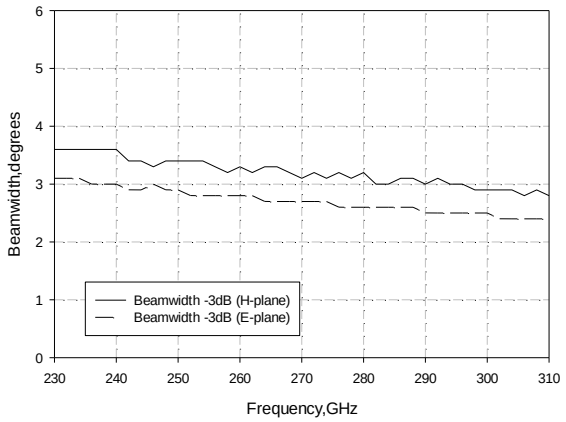

Fig. 11. Simulated 3dB beamwidth in the H- and E-planes.

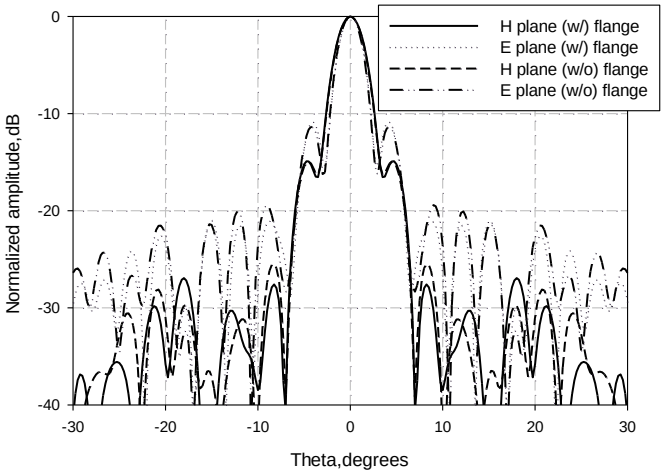

Fig. 12. Simulated normalized radiation patten comparison with and without the effect of screws and allighment pins for 290GHz.

V. Fabrication

A prototype of the proposed lens antenna has been

fabricated using CNC micromachining process. Before starting the fabrication of the lens, a jig fixture was designed and constructed from stainless steel. The fixture has been used to hold the dielectric material rod in place. This essentially resembled the waveguide flange and thus its top face was complementary to the bottom face of the lens.

To create the jig, the first operation was to turn its main body on a conventional lathe, ensuring all faces are parallel and the front mating face of jig is true and flat. The second operation was setting up the main body of the jig on the CNC milling machine to drill two dowel peg holes and whilst in this set up, drill and tap two more holes corresponding to the flange's precision screws. The last operation was to fix in two pegs and screws into jig fixture so that it would be used later to hold the lens in place.

Subsequently, the lens profile was constructed on FeatureCAM software (Delcan package) [33], with a spline tolerance of 0.015mm. This means that on the curved sections of the lens, the CNC lathe machined around the curved forms with a 0.015mm movement. When setting up the machining data for the lathe, a skim cut over the dielectric material was machined. The skimmed diameter was measured with a micrometer, which is calibrated to 0.01mm. When the lathe completed machining the lens profile, a second check was performed with a micrometer to verify the lens dome size. Finally, the lens structure was polished with Autosol paste which gives a transparent view of the lens without affecting the profile. The air pocket on the base of the dielectric lens was machined in the same setup when the holes for the alignment pins and screws were drilled (and tapped) into lens. Because this slot at the rear of the lens was only 0.2mm deep, we were able to use a 0.2mm diameter cutter which left a 0.1mm radius in corners of the rectangular slot. This is important since small micro-cutters have only a small cutting flute length which restricts how deep the cutter can machine to.

VI. Measurements

A photograph of the fabricated lens antenna is shown in Fig. 13(a). In the figure, the antenna is fitted on the WR-3 waveguide flange which enables incorporation of the antenna structure to the waveguide based system available for the measurements. Namely, the system is a Stepped Frequency Radar (SFR). The drive source of the SFR is an Agilent FieldFox portable Vector Network Analyser (VNA) operating from 2 to 18GHz. The system has a frequency range from 282GHz to 298GHz. This is generated from the RF input of 2-18GHz using a commercial mixer-based up-converter [33, 34]. Finally, the signal is mixed again to 2-18GHz using a matching down-converter. The floor and vertical walls of the room where the measurements were conducted were covered by suitable carpets which have been proven to be the most appropriate absorbers for low-THz frequencies [35].

In order to measure the antenna far field characteristics, the antenna was mounted on the transmitter (Fig. 13b). The module was placed on a metallic stage whose position can be adjusted on y- and z-axis for alignment purposes. A schematic of the measurement set up is shown in Fig. 13(c). A pyramidal horn antenna with 25dB gain and nearly 10^o beamwidth in both planes, has been used as a reference antenna at the receiver. The distance between the two antennas was set to x=3.4m, while the minimum far field distance of the lens antenna is ~1.1m. A linear positioner with 1mm accuracy has been used to measure the radiation patterns. A horizontal translation of the antenna under test (AUT) corresponds to a particular angle, which can be easily calculated from the expression $\theta_n = \arctan(y_n/x)$ (Fig.13c). The maximum scanning range is limited by the length of the positioner which is about 2m. Thus, for the particular separation distance, $\theta_{max}=16.3^o$.

Prior to the lens antenna measurement, the radiation patterns of the reference horn antenna were measured using a second identical pyramidal horn antenna. Due to the nature of our system and according to Friis equation [36], the measured radiated power is the product of the radiated power from each antenna. Hence, the radiation characteristics of the horn are calculated from the square root of the measured power. Similarly, the radiation patterns of the proposed lens antenna are calculated dividing the measured power patterns with the ones of the reference antenna. The measured H- and E-plane radiation patterns for three frequencies across the operating bandwidth are shown in Fig. 14 in comparison with the corresponding simulated patterns. A dynamic range of more than 40dB was achieved for the patterns' measurement. A good agreement has been obtained with a measured 3dB beamwidth of 3^o. The slight discrepancy observed, especially in the slidelobes, including the slight asymmetry of the patterns can be attributed to the uncertainty in the positional incursion of the metallic screws the fix the waveguide flange to the lens after these are tightened.

In Fig. 15, the measured gain is depicted together with simulated results for two different loss tangent values. These values correspond to the maximum and minimum $tan\delta$ values for rexolite within the range of 10GHz-500GHz. The frequency range of the measured gain is limited by the SFR system's range, however it does not cover the 3dB bandwidth of the lens antenna which is 30% (see Fig. 14). It can be observed that the measured realized gain is 29dB ±1dB which is just over 2dB less than the simulated one. This discrepancy can be accounted for by primarily taking into account the fact that the manufacturer quoted value for ε_r for Rexolite is claimed to be constant (ε_r=2.53) between 1MHz and 500GHz [37], which is unrealistic. At the same figure, the measured accepted gain is shown. It can be observed that while the realized gain exhibits a decreasing slope, the accepted gain agrees better with the expected response.

Finally, the S_{11} of the fabricated antenna was measured using an Agilent N5250A network analyzer with OML WR-3 extension head. The measurements were subject to a Short-Offset-Load-Offset-Load (SOLOL) calibration. The simulated and measured results are presented in Fig. 16. At the lower end of the operating frequency band both the measured and the simulated S_{11} are well below −15dB. At the upper end of the band, the measured response exhibits an increase of its level, however it remains below −14dB. The discrepancy

between simulation and measurements can be attributed to slightly different dimensions of the air pocket due to fabrication inaccuracies. This assumption is based on the study presented in Fig. 4, from which it is evident that very small changes in the height of the pocket cause differences in the S_{11} level.

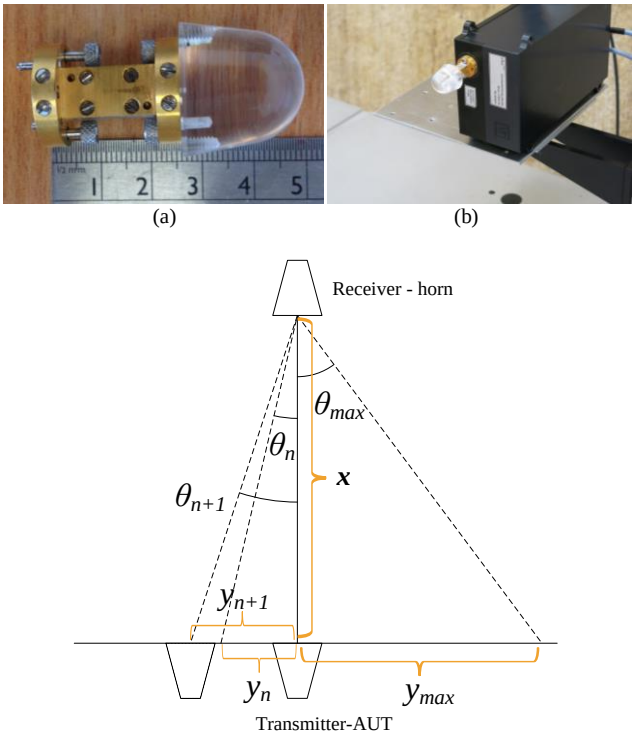

Fig. 13. Lens prototype: (a) photograph showing the lens mounted on the WR-3 flange, (b) photograph showing the whole antenna assembly mounted on the trasmittter and the linear positioner system. (c) Linear positioner geometry for measuring radiation pattern.

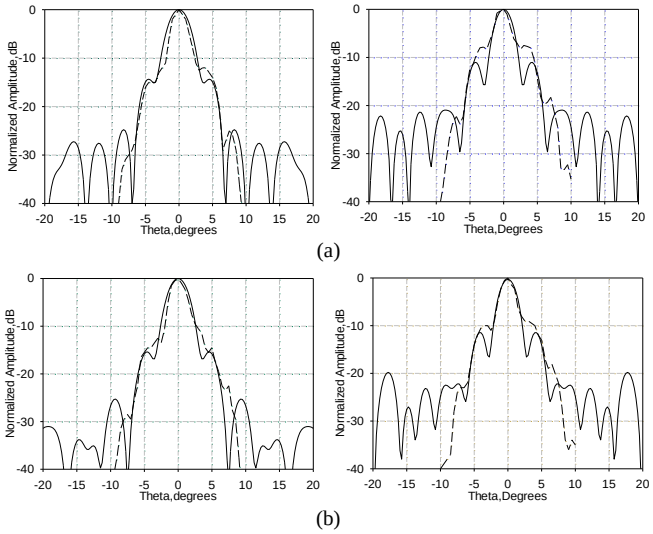

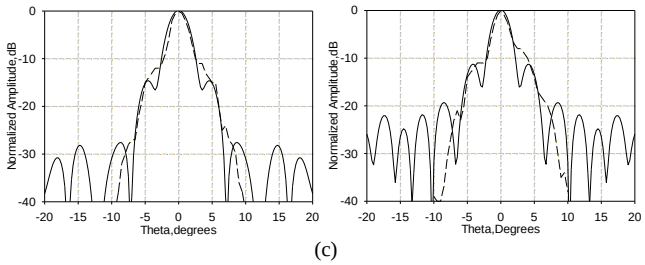

Fig. 14. Measured (dashed line) and simulated (solid line) normalized radiation patten for (a) 282GHz, (b) 290GHz and (c) 298GHz, H-plane(left), E-plane(right).

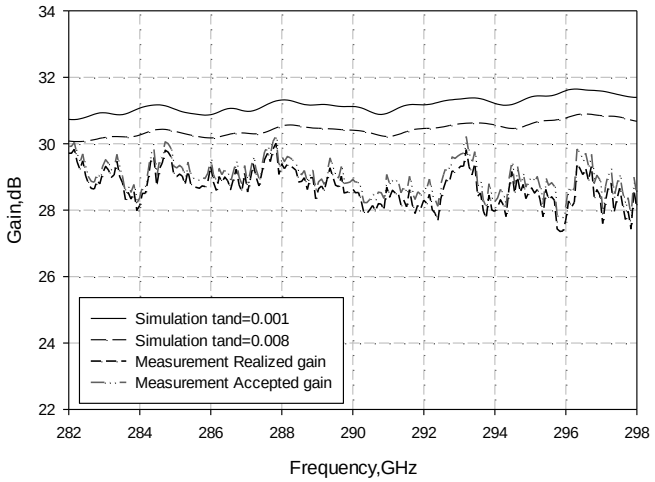

Fig. 15. Measured and simulated realized gain of the proposed lens antenna.

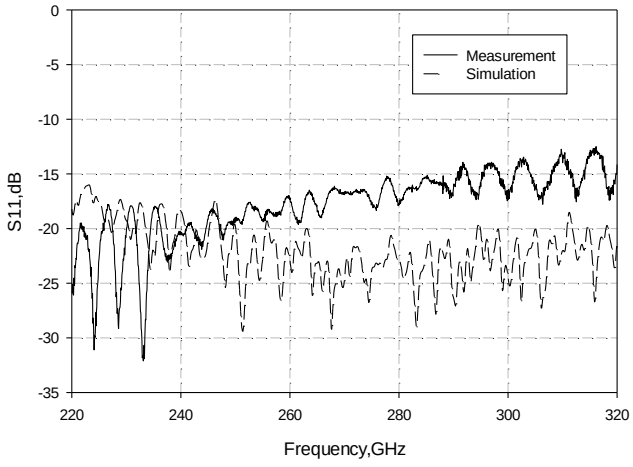

Fig. 16. Measured and simulated input reflection coefficient of the proposed lens antenna.

VII. Conclusion

In this paper, a highly directive lens antenna operating at low-THz frequencies has been proposed, with an integrated open-ended waveguide primary source. A novel matching technique based on an air pocket etched off the dielectric is employed to obtain broadband operation. An optimized

geometry based on a tapered extension is proposed which improves sidelobe level and gain performance. The achieved beamwidths (around 3º) show that the antenna can be incorporated to obtain a high-resolution imaging system. Moreover the antenna weights just 5 g and is composed of low cost material while a simple fabrication process was adopted. The antenna has an operating 3dB gain bandwidth of 30% (80GHz) achieving a maximum of 30dB measured gain. The measured S_{11} is well below -14dB across the WR-3 band. Beam scanning capabilities of such antennas at low-THz will be subject of future investigation.

ACKNOWLEDGMENT

The authors would like to thank A. Page and J. Sangha for fabrication of the lens antenna and A. Yates for his technical support and for helping in the setup of the antenna measurements.

REFERENCES

[1] R. Appleby and R. N. Anderton, "Millimeter-wave and submillimeter wave imaging for security and surveillance," *Proc. IEEE*, vol. 95, no. 8, pp. 1683–1690, Aug. 2007.

[2] H.-J. Song and T. Nagatsuma, "Present and future of terahertz communications," *IEEE Trans. Terahertz Sci. Technol.,* vol. 1, no. 12, pp. 256–263, Sep. 2011.

[3] K. B. Cooper, R. J. Dengler, N. Llombart, B. Thomas, G. Chattopadhyay, and P. H. Siegel, "THz imaging radar for standoff personnel screening," *IEEE Trans. Terahertz Sci. Technol*., vol. 1, no. 1, pp. 169–182, Jan. 2011.

[4] K. Konstantinidis, A. P. Feresidis, Y. Tian, X. Shang and M. J. Lancaster, "Micromachined terahertz Fabry–Perot cavity highly directive antennas, " *IET Microwaves, Antennas & Propagation*, vol. 9, no. 13, pp. 1436-1443, 10 22 2015.

[5] A. Jam and K. Sarabandi, "A horizontally Polarized beam-steerable antenna for sub-millimeter-wave polarimetric imaging and collision avoidance radars," presented at the IEEE Antennas and Propagation Symp., Fajardo, Puerto Rico, 2016.

[6] C. A. Fernandes, J. R. Costa, E. B. Lima and M. G. Silveirinha, "Review of 20 Years of Research on Microwave and Millimeter-wave Lenses at "Instituto de Telecomunicaçoˇes"," *IEEE Antennas and Propagation Magazine*, vol. 57, no. 1, pp. 249-268, Feb. 2015.

[7] A. V. Boriskin, R. Sauleau, and A. I. Nosich, "Performance of hemielliptic dielectric lens antennas with optimal edge illumination," *IEEE Trans. Antennas and Propag.*, vol. 57, no. 7, pp. 2193-2198, 2009.

[8] P. Otero and G. V. Eleftheriades, "Integrated modified rectangular loop slot antenna on substrate lenses for millimeter- and submillimeter-wave frequencies mixer applications," *IEEE Trans. Antennas Propag.*, vol. 46, no. 10, pp. 1489–1497, Oct. 1998.

[9] X. Wu, G. V. Eleftheriades, and T. E. van Deventer-Perkins, "Design and characterization of a single- and multiple-beam millimeter-wave circularly polarized substrate lens antennas for wireless communications," *IEEE Trans. Microw. Theory Tech.,* vol. 47, no. 6, pp. 732–737, Jun. 1999.

[10] A. P. Pavacic, D. L. del Rio, J. R. Mosig, and G. V. Eleftheriades, "Three-dimensional ray-tracing to model internal reflections in off axis lens antennas," *IEEE Trans. Antennas Propag.,* vol. 54, no. 2, pp. 604–612, Feb. 2006.

[11] N. T. Nguyen, R. Sauleau, and C. Jos Martinez Prez, "Very broadband extended hemispherical lenses: Role of matching layers for bandwidth enlargement," *IEEE Trans. Antennas Propag.*, vol. 57, no. 7, pp. 1907–1913, Jul. 2009.

[12] C. Fernandes, E. B. Lima, and J. R. Costa, "Broadband integrated lens for illuminating reflector antenna with constant aperture efficiency," *IEEE Trans Antennas Propag.*, vol. 58, no. 12, pp. 3805–3813, 2010.

[13] R. Sauleau and B. Bares, "A complete procedure for the design and optimization of arbitrarily shaped integrated lens antenna," *IEEE Trans. Antennas Propag.*, vol. 54, no. 4, pp. 1122–1133, Apr. 2006.

[14] G. Godi, R. Sauleau, L. Le Coq, and D. Thouroude, "Design and optimization of three dimensional integrated lens antennas with genetic algorithm," *IEEE Trans. Antennas Propag.*, vol. 55, no. 3, pp. 770–775, Mar. 2007.

[15] H. Sherry et al., "Lens-integrated THz imaging arrays in 65 nm CMOS technologies," in *Proc. IEEE RFIC*, 2011, pp. 1–4.

[16] N. Sarmah *et al*., "A Fully Integrated 240-GHz Direct-Conversion Quadrature Transmitter and Receiver Chipset in SiGe Technology," *IEEE Transactions on Microwave Theory and Techniques*, vol. 64, no. 2, pp. 562-574, Feb. 2016.

[17] D. F. Filipovic, S. S. Gearhart, and G. M. Rebeiz, "Double-slot antennas on extended hemispherical and elliptical silicon dielectric lenses," *IEEE Trans. Microw. Theory Tech*., vol. 41, no. 10, pp.1738–1749, Oct. 1993.

[18] A. D. Semenov, H. Richter, H.-W. Hübers, B. Günther, A. Smirnov, K. S. Il'in, M. Siegel, and J. P. Karamarkovic, "Terahertz performance of integrated lens antennas with a hot-electron bolometer," *IEEE Trans. Antennas and Propag*., vol. 55, no. 2, pp. 239–247, Feb. 2007.

[19] J. Montero-de-Paz, E. Ugarte-Munoz, L.E. Garcia-Munoz, I. Camara Mayorga, D. Segovia-Vargas, "Meander Dipole Antenna to Increase CW THz Photomixing Emitted Power, " *IEEE Trans. Antennas Propag.,* vol.62, no.9, pp.4868-4872, Sept.2014.

[20] N. Llombart, G. Chattopadhyay, A. Skalare, and I. Mehdi, "Novel terahertz antenna based on a silicon lens fed by a leaky wave enhanced waveguide," *IEEE Trans. Antennas Propag.,* vol.59, no.6, pp.2160–2168, Jun. 2011.

[21] D. F. Filipovic, G. P. Gauthier, S. Raman, and G. M. Rebeiz, "Off-axis properties of silicon and quartz dielectric lens antennas," *IEEE Trans. Antennas Propag.*, vol. 45, no. 5, pp. 760–766, May 1997.

[22] CST Microwave Studio [Online]. Available: http:// www.cst.com/.

[23] M. J. M. van der Vorst, P. J. I. de Maagt, A. Neto, A. L. Reynolds, R. M. Heeres, W. Luingue, and M. H. A. J. Herben, "Effect of internal reflections on the radiation properties and input impedance of integrated lens antennas—Comparison between theory and measurements," *IEEE Trans. Microwave Theory Tech.,* vol. 49, no. 6, pp. 1118–1125, Jun. 2001.

[24] A. Neto, N. Llombart, J.J.A. Baselmans, A. Baryshev, and S.J.C. Yates, "Demonstration of the leaky lens antenna at submillimeter wavelengths," *IEEE Trans. Terahertz Sci. Technol.*, vol. 4, no. 1, pp. 26-32, Jan 2014.

[25] A. J. Alazemi, H. H. Yang and G. M. Rebeiz,, "Double Bow-Tie Slot Antennas for Wideband Millimeter-Wave and Terahertz Applications," *IEEE Trans. Terahertz Sci. Technol.*, vol. 6, no. 5, pp. 682-689, Sep. 2016.

[26] O. Yurduseven, N. Llombart and A. Neto, "A Dual-Polarized Leaky Lens Antenna for Wideband Focal Plane Arrays," *IEEE Trans. Antennas Propag.*, vol. 64, no. 8, pp. 3330-3337, Aug. 2016.

[27] A. Garufo and N. Llombart and A. Neto, "Radiation of Logarithmic Spiral Antennas in the Presence of Dense Dielectric Lenses," *IEEE Trans. Antennas Propag.*, vol. 64, no. 10, pp. 4168-4177, Oct. 2016.

[28] J.M. Edwards, R. O'Brient, A.T. Lee, and G.M. Rebeiz, "Dual-polarized sinuous antennas on extended hemispherical silicon lenses," *IEEE Trans. Antennas Propag.*, vol. 60, no. 9, pp. 4082-4091, Sep. 2012.

[29] D. R. Vizard, M. Gashinova, E. G. Hoare, M. Cherniakov, "Low THz automotive radar developments employing 300–600 GHz frequency extenders," *16th International Radar Symposium (IRS)*, pp.209-214, June 2015.

[30] J. Ala-Laurinaho, J. Aurinsalo, A. Karttunen, M. Kaunisto, A. Lamminen, J. Nurmiharju, A.V. Räisänen, J. Säily, and P. Wainio, "2-D beam-steerable integrated lens antenna system for 5G E-band access and backhaul," *IEEE Trans. Microw. Theory Tech.*, vol. 64, no. 7, pp. 2244-2255, July 2016

[31] M. J. M. van der Vorst, P. J. I. de Maagt, and M. A. J. Herben, "Effect of internal reflections on the radiation properties and input admittance of integrated lens antennas," *IEEE Trans. Microw. Theory Tech.,* vol. 47, no. 9, pp. 1696–1704, Sep. 1999.

[32] A. Karttunen, J. Ala-Laurinaho, R. Sauleau, and A. V. Räisänen, "Reduction of internal reflections in integrated lens antennas for beam-steering," *Progress In Electromagnetics Research*, vol. 134, pp. 63-78, 2013.

[33] Retrieved from www.delcam.com/software/featurecam/

[34] Retrieved from www.vivatech.biz

[35] A. Lonnqvist, A. Tamminen, A. V. Räisänen, "Monostatic Reflectivity Measurement of Radar Absorbing Materials at 310 GHz," *IEEE Transactions on Microwave Theory and Techniques*, Vol. 54, No. 9, pp. 3486-3491, Sept. 2006.

[36] C. A. Balanis, "*Antenna Theory: Analysis and Design*," Second edition, New York: John Wiley & Sons Inc, 1997.
[37] Retrieved from http://www.rexolite.com/specifications/